Patchy cleaning of rigid gas filters—transient regeneration phenomena comparison of modelling to experiment

Achim Dittler [a,*], Martin V. Ferer [b], Pulkit Mathur [b], P. Djuranovic [b], Gerhard Kasper [a], Duane H. Smith [b,c]

[a] *Institut für Mechanische Verfahrenstechnik und Mechanik, Universität Karlsruhe (TH), D-76128 Karlsruhe, Germany*
[b] *Department of Physics, West Virginia University, P.O. Box 6315, Morgantown, WV 26506-6315, USA*
[c] *National Energy Technology Laboratory (NETL), U.S. Department of Energy, P.O. Box 880, Morgantown, WV 26507-880, USA*

Abstract

Rigid ceramic filter media, widely used for the removal of particles from gas streams at elevated temperatures tend to show patchy cleaning when the filter regeneration is incomplete [Filtr. Sep. (1989) 187]. In order to investigate the regeneration behaviour and the operational performance of partially regenerated, rigid gas cleaning filter media over many filtration cycles, experiments were performed in a filter test rig. The regeneration behaviour of the filter sample was characterized by the overall regeneration efficiency, the local frequency of regeneration, and the number and size of regenerated filter areas. Using only four adjustable parameters, our modelling results compare favourably with our experimental results, at room temperature. This favourable comparison of the regeneration behaviour between modelling and experiment is achieved only if it is assumed that cohesive and adhesive bonds, which are broken during filter regeneration, do not heal during the next filtration cycle. Assuming otherwise would cause (i) the dust cake to be removed at the same positions during every regeneration and (ii) the patch size to increase from cycle to cycle instead of decreasing as seen in the experiment. Therefore, the model development was guided by our extensive experimental results. This agreement of modelling with experiment indicates that the modelling has real predictive capabilities for operational filter cleaning. Both filter conditioning and dust cake compression significantly influence the operational performance of partially regenerated filter media.

1. Introduction

Surface filters are one of the options for particulate removal from gas streams. During the filtration process, filter cake builds up on the surface of the filter medium, and the overall pressure drop of the filter medium increases. In order to maintain an economical filtration process, the filter media need to be regenerated. This is usually accomplished by pulse-jet regeneration. Besides mechanical failure of the filter medium itself, patchy, incomplete regeneration [1] is one of the main problems encountered when regenerating the filter media. Incomplete filter regeneration significantly influences the operational performance of the filter media: the lower the regeneration efficiency, the shorter the filter cycle times and the more frequently the filter needs to be regenerated. In extreme cases, the filter operation is not stable and the filtration process collapses.

Besides dust cake adhesion to the filter surface [5] and operating conditions (e.g., the humidity [7]), the cohesive strength of the dust cake [6] and the structure of the filter medium itself affect the regeneration behaviour of the filter medium. A few studies have modelled the regeneration behaviour for complete filter regeneration on a two-dimensional microscopic basis [8,9]. Besides these, other authors report a probabilistic model based on random local filter regeneration [2–4]. First attempts to compare measured data of the adhesion of a particle layer [15] with results from a physically based model taking into account local adhesive and cohesive strengths of the dust cake were reported by Ferer and Smith [16]. However, thus far there is no direct comparison of modelling results with experimental data for transient regeneration phenomena of sur-

* Corresponding author. Present Address: DaimlerChrysler AG, FTK/A, HPC G206, 70546 Stuttgart, Germany. Tel.: +49-711-17-53967; fax: +49-711-17-24460.
E-mail address: achim.dittler@daimlerchrysler.com (A. Dittler).

face filters (i.e., the development of regeneration efficiency, local regeneration frequencies, patch size distributions, etc. over a series of filtration cycles).

This contribution compares modelling results to experimental values for incompletely regenerated, rigid filter media. The experiments on transient development of regeneration efficiency, local regeneration frequency and patch size distribution as well as the operational behaviour were performed under ambient conditions in a lab-scale filter test rig. In comparing the results of the independent modelling to these data, only four parameters were adjusted. The comparison of the modelling results to experiment provides insight into the reasons for patchy cleaning and shows the influences of cohesive and adhesive bonds as well as of the regeneration parameters on the patchy cleaning patterns, on the local frequency of regeneration, and on the overall regeneration efficiency over a series of filtration cycles. Lastly, the influence of the regeneration behaviour on the operational performance is discussed.

2. Experimental procedure

2.1. Filter test rig

The experimental investigations performed within the scope of the present contribution are carried out in a lab scale filter test rig which is built according to German VDI guideline 3926 [26]. Fig. 1 is a schema of the test rig. It mainly consists of a vertical crude gas channel and a horizontal clean gas extraction tube. The filter coupon (15-cm diameter) under investigation is mounted parallel to the crude gas channel which enables cross-flow filtration as experienced in real filter housings.

Besides the photometric concentration monitor and the control device, an optical measuring system is mounted on the filter test rig opposite the filter coupon. This measuring system, described in detail in Ref. [10], enables the full-field

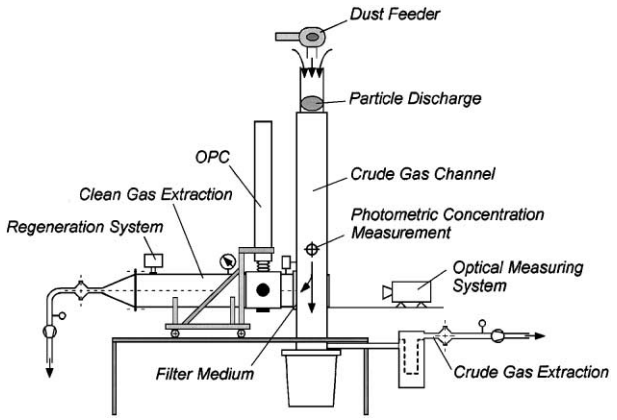

Fig. 1. Lab Scale Filter Test Rig [26].

in situ measurement of the dust cake height distribution on the surface of the filter medium. From these measurements, we obtain the overall frequency of regeneration as well as the local frequencies of regeneration and the patch size distribution, as discussed later. In addition, we investigate the influence of the regeneration behaviour on the filtration performance (time dependence of filtration cycle times and residual pressure drop) of the filter medium.

2.2. Operational conditions

The experimental investigation of the transient regeneration behaviour was performed with a fibrous ceramic filter medium to remove quartz dust from the 'dirty' gas. The filtration experiment was performed under ambient temperature with a filtration velocity of $v = 5$ cm/s. The filter medium was regenerated by a pulse of compressed air ($p_t = 2{,}5$ bar, $t_{valve} = 50$ ms) when the maximum pressure drop of 2100 Pa was reached. After the filter regeneration the dust cake height profile was measured and the local and overall regeneration efficiency was determined in accordance to the procedure described below. From the cleaning pattern, we obtained the number of regenerated filter areas as well as their size and location. In addition to these measurements of regeneration behaviour, the residual pressure drop and the cycle time were measured to characterize the operational behaviour of the filter medium.

2.3. Experimental determination of regeneration efficiency, local frequency of regeneration and patch size distribution

Several attempts based on different methods have been reported for determining the regeneration efficiency of gas cleaning filters. One method determines the regeneration efficiency by measuring the mass of the filter before cleaning and the mass released from the filter medium. This gives a mass-related regeneration efficiency [27]. Another method obtains the regeneration efficiency indirectly from the resistance to flow of the incompletely regenerated filter medium, as given by Cheung [28]. Kanaoka et al. [29] who calculate the regeneration efficiency from the operational data for the pressure drops across a new filter as compared with later cycle data for the pressure drops before and after regeneration. Operational filtration data were compared with fitting equations from a parametric model by Smith et al. [32,33]. Regardless of the physical basis on which the regeneration efficiency is obtained, all these methods give an overall regeneration efficiency. Therefore, these methods cannot be used to determine local regeneration efficiencies or local frequencies of regeneration. To measure local frequencies of regeneration, the regeneration of a particular area is determined as follows:

A threshold height value is defined. Regions with dust cake heights below the threshold value are considered to be regenerated, while regions with heights above the

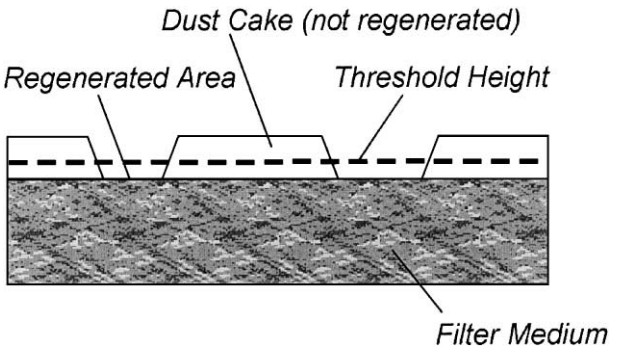

Fig. 2. Schematic of filter/filter-cake cross-section showing the threshold height for determination of local regenerations.

threshold value are considered to be unregenerated. Fig. 2 illustrates the procedure schematically. On the left-hand side (a) of Fig. 3, one can see the grey value encoded height profile of the dust cake after the very first regeneration.

The very dark grey regions represent dust cake, which was lifted from the surface (adhesive bonds broke) but not removed. The dust cake has been removed from the filter medium in the white regions. On the right-hand side, Fig. 3b), the threshold procedure gives the patchy cleaning pattern, from which we obtain the local frequency of regeneration, the overall regeneration efficiency and the patch size and number. The local frequency of regeneration is obtained by summing up the regeneration efficiencies obtained locally over a number of filtration cycles, whereas the overall regeneration efficiency is simply the ratio of the white area to the total filter area. Patch size and number of patches are a result of image analysis performed with the NIH Image.

3. Fine-scale model of transient regeneration

In the physical system, which originally motivated this model, a layer of filter cake is deposited on a cylindrical candle filter to some thickness, t; then a backpulse of compressed air is applied from the inside of the candle filter to blow-off the filter cake, thus cleaning the filter. The force actually responsible for removing the layer of filter cake is due to the pressure drop, ΔP, across the layer. As shown in Fig. 4, the model cylinder is cut along a seam and then flattened in the xy plane. Periodic boundary conditions connecting the $y=0$ and $y=L$ sides preserve the continuity around the cylinder. Of course, the planar filter in the model more closely mimics the present, experimental filter system.

We present a brief overview of our basic model, which has been fully described elsewhere [18–22]. In our model, the layer is gridded into rectangular blocks, of base ℓ^2 and height $T\ell$, connected to the filter and to each other by spring like forces. The applied backpulse pressure force, $F=\Delta P\ell^2$, will be balanced by the adhesive and cohesive spring forces (with spring constants k^{a} and k^{c}, respectively). Eq. (1) shows the force balance between the applied force F on a block at $\vec{r}=(1/2)(i,j)$ (i and j are even integers determining the location along the x- and y-directions, respectively) and the spring-like forces as depending on the displacements of that block and the surrounding blocks:

$$F = k^{\mathrm{a}}_{i,j}\varepsilon_{i,j} - \left\{k^{\mathrm{c}}_{i-1,j}(\varepsilon_{i-2,j}-\varepsilon_{i,j}) + k^{\mathrm{c}}_{i+1,j}(\varepsilon_{i+2,j}-\varepsilon_{i,j}) + k^{\mathrm{c}}_{i,j-1}(\varepsilon_{i,j-2}-\varepsilon_{i,j}) + k^{\mathrm{c}}_{i,j+1}(\varepsilon_{i,j+2}-\varepsilon_{i,j})\right\}. \quad (1)$$

These spring constants are chosen randomly from particular probability distributions so that the average stiffness of the adhesive springs is 1/2, and the average stiffness of the cohesive springs is $T/2$($\langle k^{\mathrm{a}}\rangle = 1/2$ and $\langle k^{\mathrm{c}}\rangle = T/2$). This thickness parameter, T, gives the ratio of average cohesive to average adhesive strength [18–20].

Given the distributions of stiffnesses and the value of the force, F, we perform Gauss–Seidel iterations to determine the displacements. If any adhesive spring is stretched beyond its strength, S^{a}, that spring will break; similarly, if

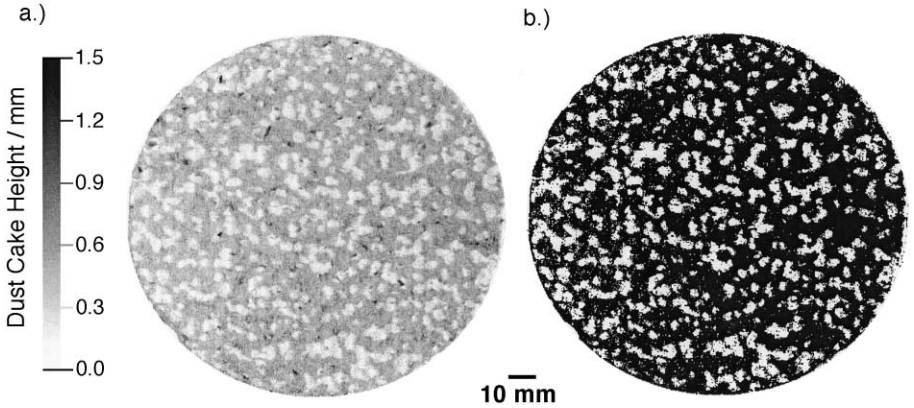

Fig. 3. (a) Grey scale encoded dust cake height profile; the threshold procedure gives the patchy cleaning pattern shown in (b) on the right (white patches are cleaned).

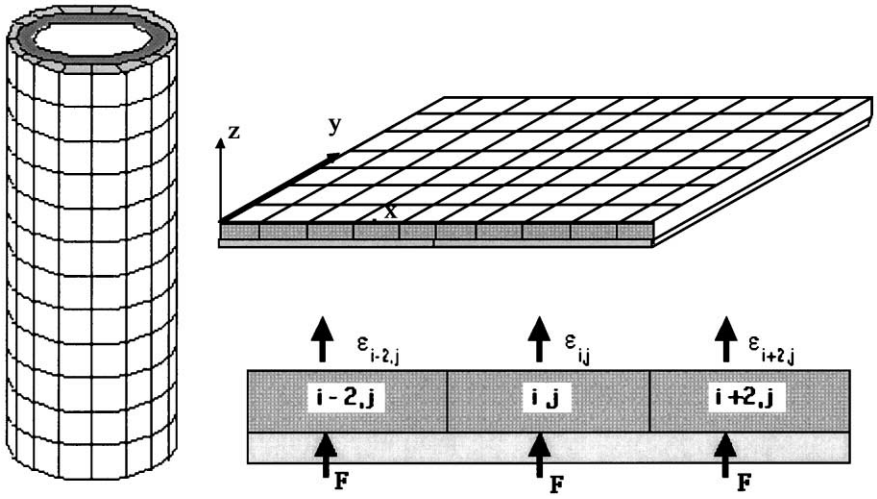

Fig. 4. Imaginary gridding of the filter cake on the surface of the filter.

any cohesive spring is stretched beyond its strength, S^c, i.e.

$$k^a_{i,j}\varepsilon_{i,j} > S^a_{i,j} \quad \text{and} \quad k^c_{i,j+1}\,|\,\varepsilon_{i,j} - \varepsilon_{i,j+2}\,| > S^c_{i,j+1}, \tag{2}$$

that cohesive spring will break. The strengths are chosen so that the average value of the strength of the adhesive springs is given by $\langle S^a\rangle = 1/2$ and so that the average value of the strength of the cohesive springs is given by $\langle S^c\rangle = T/2$. This model is similar to many models of quasi-static, tensile fracturing in the scientific literature [23–25].

In a previous work on this model, the primary focus was the thickness dependence of the backpulse cleaning of a uniformly heterogeneous layer. To study the actual operational behaviour, it is essential to characterise the filter-cake redeposition on the patchily cleaned filter surface from one cycle to the next. This adds a number of features affecting the backpulse cleaning, which were not included in the previous modelling, as follows.

(i) The thickness of the filter cake will no longer be uniform due to added deposition on uncleaned regions.

(ii) Uncleaned patches that were raised from the filter surface during cleaning will not re-adhere as strongly to the filter surface during the next filtration cycle.

(iii) Cracks through the filter cake layer will not completely heal during filtration, i.e. broken cohesive bonds between blocks which were not removed will not reform to their original strength.

(iv) Filter cake compression will make uncleaned patches less porous and stronger than newly deposited patches.

(v) There will be a reduction in permeabilities and an increase in the total pressure drop because of filter surface conditioning, in which a thin layer of filter cake has penetrated deep enough into the surface of the filter to be uncleaned during the backpulse.

In depositing the filter cake on a patchily regenerated surface, as in item (i) above, we assume that the flow velocity through any unit area of the surface is proportional to a permeability for that area. For any unit area

$$\Delta P = K_1'\, v + K_2'\, Wv, \tag{3}$$

where v is the filter face velocity during filtration (e.g., $v = 5$ cm/s), K_1' is the total specific flow resistance of the filter (e.g., $K_1' = 3000$ Pa/(m/s)), K_2' is the specific flow resistance of the filter cake (e.g., $K_2' = 120{,}000$ l/s) and W is the areal mass loading. Being the mass of cake deposited upon a unit area of the filter, the areal mass loading is simply proportional to the thickness t:

$$W = \rho_s(1-\varepsilon)t, \tag{4}$$

where ρ_s is the density of the solid particles and ε is porosity. For the experimental parameters [12], $\rho_s = 2700$ kg/m^3 and $\varepsilon = 0.8$; defining thickness $t = T$ mm, we find a flow resistance per mm of thickness $K_2' W = 648T$ Pa/(cm/s). These enable a determination of the resistance to flow (v), r_f for the filter and $r_c T$ for thickness T mm of the cake:

$$\Delta P = K_1'\, v + K_2'\, Wv = r_f v + r_c T v = r_c(R+T)v, \tag{5}$$

where R is the dimensionless ratio of flow resistances, $R = r_f/r_c$ (using experimental parameters $R = 0.046$, $v = v$ cm/s, $r_c = 648$ Pa).

In this version of the filter cake removal model, we assume a 'bundle-of-tubes' type flow, where the flow resistance is perpendicular (no cross-flow) through any one block (i,j) of area A, so that flow resistance is given by the flow resistance of that block located at $r = (i,j)$

$$v_{(i,j)} = (\Delta P/r_c)/(R + T_{(i,j)}). \tag{6}$$

Although it has been shown that horizontal flows can be important [12], this simple approximation will give an estimate of the real filter-cake height variations occurring as the filtration/cleaning process is cycled. Furthermore, we assume that the pressure drop is uniform over the surface.

In filtration, the average flow velocity is constant (e.g., $v=5$ cm/s, $v=5$). We equate our average volume flow velocity $\langle q_{(i,j)}\rangle$ to the constant volume flow velocity q_{f}, and therefore the average velocity to the constant velocity, $v_{\mathrm{f}}=5$,

$$\langle v_{(i,j)}\rangle = (\Delta P/r_{\mathrm{c}})\left\langle (R+T_{(i,j)})^{-1}\right\rangle = v_{\mathrm{f}}. \tag{7}$$

This determines the filtration pressure drop as a function of time

$$\Delta P(t) = r_{\mathrm{c}} v_f / \left\langle (R+T_{(i,j)})^{-1}\right\rangle, \tag{8}$$

in terms of the constants, r_{c}, R, and v_{f} and of the distribution of thicknesses, $T_{(i,j)}$ at time t. In turn, Eqs. (6) and (8) can be used to determine the flow velocity through block (i,j) at time t:

$$v_{(i,j)} = \left(v_{\mathrm{f}}/\left\langle (R+T_{(i,j)})^{-1}\right\rangle\right)/(R+T_{(i,j)}); \tag{9}$$

and therefore, the rate of filter cake deposition on block (i,j) at time t is given by:

$$\begin{aligned} A\left(\frac{\mathrm{d}T_{(i,j)}(t)}{\mathrm{d}t}\right) &= \eta q(i,j) = A\eta v_{(i,j)} \\ &= A\eta\left(v_{\mathrm{f}}/\left\langle (R+T_{(i,j)})^{-1}\right\rangle\right)/(R+T_{(i,j)}), \end{aligned} \tag{10}$$

where A is the cross-sectional area of one block, and where η is the number of cubic millimeters of filter cake deposited per unit volume of gas filtered. Integrating Eq. (10) from the time immediately after cleaning, t_{o}, to the end of the filtration cycle at some final time, t_{f}, one determines the thickness distribution, each $T_{(i,j)}$, after the filtration cycle

$$\begin{aligned} T_{(i,j)}(t_{\mathrm{f}}) &= T_{(i,j)}(t_{\mathrm{o}}) + \int_{t_{\mathrm{o}}}^{t_{\mathrm{f}}} \frac{\mathrm{d}T_{(i,j)}(t)}{\mathrm{d}t}\,\mathrm{d}t = T_{(i,j)}(t_{\mathrm{o}}) \\ &\quad + \int_{t_{\mathrm{o}}}^{t_{\mathrm{f}}} \frac{\nu_{\mathrm{f}}\eta}{\left\langle (R+T_{(i,j)})^{-1}\right\rangle (R+T_{(i,j)})}\,\mathrm{d}t, \end{aligned} \tag{11}$$

where the final time is to be determined by operating conditions, e.g., (i) if the filtration ends at t_{f}, when the pressure reaches the same maximum value at the end of every cycle, or (ii) if the filtration ends at the same t_{f} for every cycle.

Having determined the thickness distribution after filtration, we assign values of cohesive bonds between any two blocks based upon the block with the minimum thickness. However, the procedure is different, if there is a broken cohesive bond (i.e., if there is a broken cohesive bond between two blocks which were not removed); the cohesive bond is only formed between the additional deposition on these two blocks. The deposition described above provides a simple but hopefully accurate approximation to the actual filter cake deposition. Our results agree with the theoretical predictions of Dittler and Kasper [12,13].

In feature (ii) of the model, it was observed that numerous patches of filter cake are lifted but not removed during backpulse cleaning. It seems reasonable that these patches will not significantly re-adhere during a subsequent filtration cycle because that part of the surface is shielded during new deposition. Therefore, these patches which are lifted but not removed will be more weakly attached, so that they can be more easily removed during the next cycle. This effect has been directly observed in the experiments of Dittler and Kasper [14]. In our model, we assume no re-attachment of those blocks of filter-cake which were lifted but not removed. If the blocks had re-attached with their original strength, the filter cake would be essentially the same after each filtration cycle, so that essentially the same blocks would be removed during each regeneration, making the frequency of regeneration dramatically different from that observed experimentally.

Since many of the properties of interest depend sensitively upon the regeneration efficiency, it is important for any modelling runs to correctly reproduce the regeneration

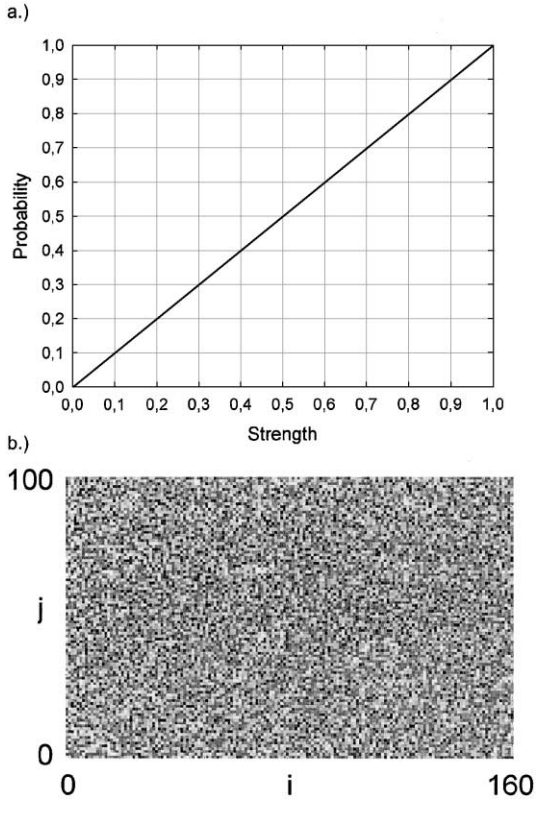

Fig. 5. (a) Cumulative distribution of bond strengths and (b) spatial distribution of adhesive strengths in the model, the strongest bonds are the darkest.

efficiency from one cycle to the next. This takes some care because the experimental efficiency depends upon any number of operating conditions (notably filter-cake compression and conditioning of the filter surface) which are difficult to characterise accurately enough to input into a model for predicting the regeneration efficiency.

The consequences of filter-cake compression include a reduction in porosity and the related strengthening of both the adhesive and cohesive bonds in the filter cake. The consequences of filter-surface conditioning include a decrease in effective filter permeability and resulting increases in pressures and filtration efficiency. These can be incorporated into the model by adjusting the adhesive and cohesive forces as well as the backpulse pressure force.

In the model used here, we assumed that the adhesive bonds are distributed randomly on the surface of the filter medium. Fig. 5a shows the cumulative distribution of bond strengths. Fig. 5b shows the local adhesive strength in the 160×100 blocks grid used. As one can see from Fig. 5b, there is a random distribution of adhesive bonds on the surface of our filter medium.

4. Comparison of modelling and experimental results

The basic purpose of this section is to determine what rules for filter-cake deposition in the model will give the best agreement with experiment. We also determine the best values of the four adjustable parameters used in the model.

4.1. Regeneration behaviour

In attempting to compare the modelling results with experiment, it was necessary to be able to reproduce the cycle-to-cycle regeneration efficiency. This involved a proper choice of backpulse cleaning force. More subtly, it was important to mimic the filter cake compression and filter-surface conditioning (points 'iv' and 'v' in the earlier discussion), which would most noticeably change the filter-cake strength and backpulse cleaning force and consequently the filter regeneration for the first few cycles. Filter conditioning reduces the permeability of the filter causing a smaller pressure drop across the filter cake after the first few cycles; therefore, the actual backpulse cleaning force decreases during the first few cycles. On the average, filter cake compression will strengthen the filter cake during the first few cycles, because a more-compact, less porous medium is stronger than a less compact medium. One would, therefore, expect that the average adhesive and cohesive strengths would increase above their initial values of 1/2 and $T/2$, respectively. If both average strengths increased by a factor of γ to the values $\gamma/2$ and $\gamma T/2$, the ratio of pressure drop to average forces would be a factor of γ smaller, although the ratio of the cohesive to adhesive strengths would remain unchanged at the value T.

Therefore, both filter conditioning and filter cake compression have the effect of decreasing the ratio of removal pressure (pressure drop across the filter cake) to average adhesive force after the first few cycles. In a simple attempt to mimic both effects, filter cake compression (point 'iv') and conditioning of the filter medium surface (point 'v'), we have introduced an 'ad-hoc' reduction in the strength of the backpulse pressure force relative to the average filter cake strengths, as the modelling proceeds from one cleaning cycle to the next. In practice, we kept the average adhesive strength fixed at the value of 1/2 and introduced a rather sharp decrease in the maximum backpulse pressure $0.275\,(1.0+(1.1/5^n))$, for cleaning cycle n. Of course, the backpulse pressure pulse exerts a cleaning pressure, which decreases from the maximum value as the average thickness of the filter cake decreases during each cleaning cycle. This expression for the maximum pressure, the first of the four adjustable parameters, gave good qualitative agreement with experimental regeneration efficiencies from cycle to cycle. Without this reduction factor, the modelling would always predict less cleaning in the first cycle than in any subsequent cycle; numerous experiments show more efficient cleaning during the first one or two cycles than during subsequent cycles. This can be understood in terms of the weaker, uncompressed filter cake during the first one or two cycles and in terms of the higher permeability of the virgin filter causing a higher removal pressure (pressure drop across the filter cake) during the first few cycles.

Fig. 6 shows the regeneration efficiency from this modelling, decreasing from approximately 32% in the first cycle to approximately 27% in the last cycles. As illustrated in Fig. 6, this agrees well with experimental results, which typically show such a decrease from the first few cleaning cycles to later cycles. The differences in the first two cycles would have been reduced by a slightly smaller decrease in the relative strength.

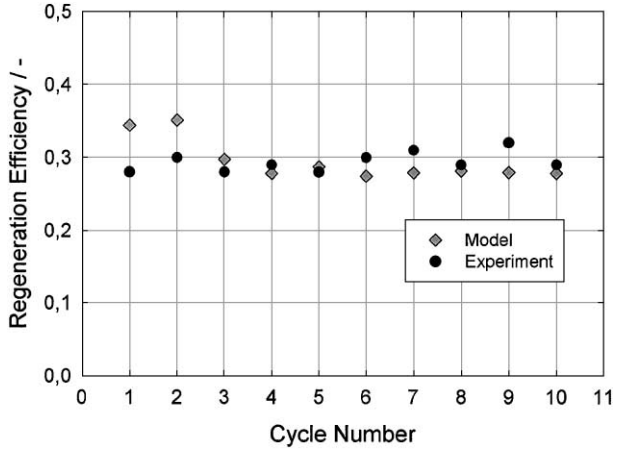

Fig. 6. Comparison of the regeneration efficiency from the modelling with the efficiency from experiment.

4.2. Frequency of regeneration

To achieve agreement with remainder of the experimental results, it was necessary to invoke feature 'iii', from Section 2.2. In an earlier version of the modelling [16], we had assumed that all of the broken cohesive bonds had reformed to their full strength characterised by the new thicknesses. With this assumption the modelling results were radically different from the experimental results. In the modelling to be discussed, we assumed that for any broken cohesive bond between two blocks, neither of which were removed, only the newly deposited filter cake formed a cohesive bond and that no fraction of the broken cohesive bond between the previously deposited filter cake was re-formed (healed).

To illustrate these rules, Fig. 7 shows a cross-section of the filter and filter cake (newly deposited filter cake is shaded darker grey). As in the actual model, more new filter cake is deposited on cleaned areas (e.g., the second block) than on the thicker, existing layers (especially the first and last blocks). There was a broken adhesive bond between the filter and the fourth block, and a broken cohesive bond between this fourth block and the fifth block. The model assumes that this adhesive bond (adhesive bonds are shown by a series of vertical lines) was not reformed upon the deposition of new filter cake during filtration. The model assumes that a cohesive bond (series of horizontal lines) is only formed by the new filter cake deposition between the fourth and fifth blocks. The cohesive bonds connecting the second block to its neighbours are weaker because the thickness associated with the bond strength between two blocks is determined by the thinner of the two blocks.

In comparing the frequencies of regeneration from the modelling with those from experiment. It is clear the agreement, although not perfect, is reasonably good. Fig. 8a gives the Portion of Surface vs. Frequency of Regeneration after 10 filter cycles.

In the modelling, 28% of the blocks are never removed (vs. 26% from experiment); 16% are removed only once (vs. 18% from experiment), etc. until 7.5% are removed 10 times (vs. 5% from experiment). Fig. 8b gives the local frequency of regeneration corresponding to Fig. 8a.

The local frequency of regeneration distributions look very similar when one adjusts for the difference in scale: the round filter coupons are 14 cm in diameter while the model filter rectangles are 10.27×6.4 cm. It is instructive to contrast this version of the model with the early version that healed all broken cohesive bonds. In the early version, 55% of the blocks were never removed; 12% were removed once; 6% were removed twice; and so forth. Because 55% of the blocks remained in place for all 10 cycles the local frequency of regeneration plots had much more white space than the result on the right of Fig. 8b). Therefore, the modelling provides results in much better agreement with experiment when the broken cohesive bonds are not restored.

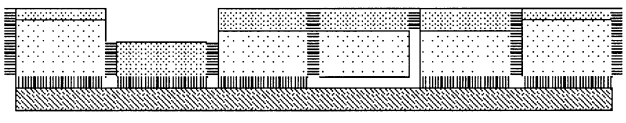

Fig. 7. Cross-section of the filter cake after a later filtration cycle. The vertical lines represent adhesive bonds; the horizontal lines represent cohesive bonds; the darker grey shading shows newly deposited filter cake.

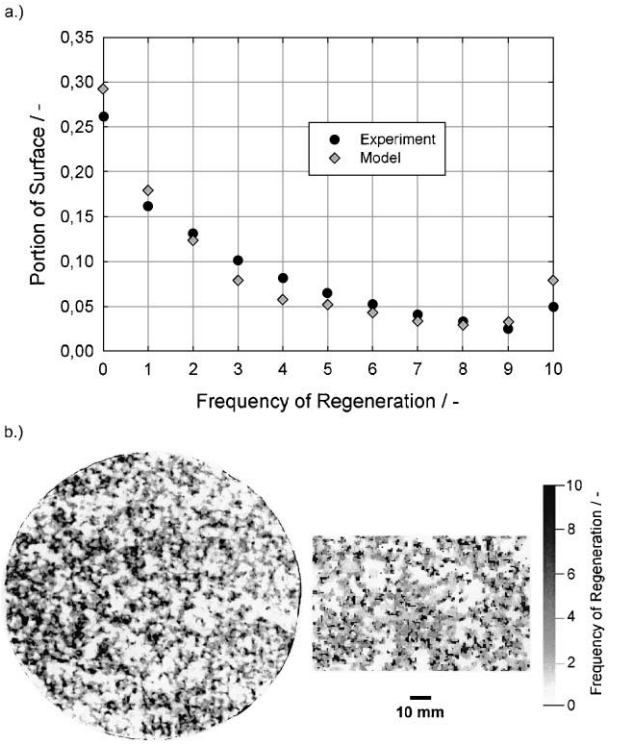

Fig. 8. (a) Frequency of regeneration plot showing the fraction of the surface cleaned zero times, once during 10 cycles, twice and so forth. (b) Local frequency of regeneration. The darkest regions are cleaned all 10 cycles; the lighter grey regions are cleaned once. The size of the modelling results, on the right, is scaled to the physical size of the experimental results as discussed in the next section.

4.3. Patch size

If one (i) chooses the value of the adjustable thickness parameter, $T = 0.5$, and (ii) scales the modelling system, so that each of the 16,000 blocks has an area $A = \ell^2 = 0.4$ mm^2, so that one of the 100×160 block model systems corresponds to a size of 10.27×6.4 cm, then the modelling results for patch size agree well with experiment. In determining the value of T and the physical size of the blocks, the second and third of the four adjustable parameters are determined. Fig. 9 gives the patch size distribution obtained from the experiment (a) and from our modelling (b).

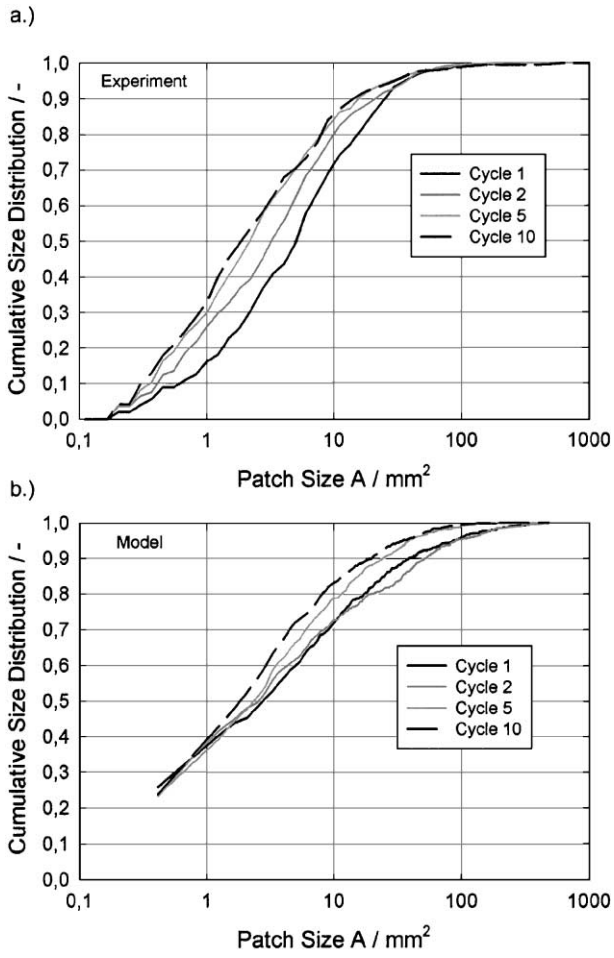

Fig. 9. (a) Cumulative patch size distribution from experiment and (b) from modelling.

When comparing the patch size distributions obtained, one can see that both, experiment and modelling, show the same tendencies. First, for the chosen thickness, $T = 0.5$, in the tenth cycle, approximately 39% of the patches have an area less than 1 mm^2 (vs. 35% from experiment) and 84% of the patches have an area less than 10 mm^2 (vs. 86% from experiment). This agreement is very sensitive to the value of T. For $T = 0.6$, 35% of the patches have an area less than 1 mm^2, while only 75% of the patches have an area less that 10 mm^2 (in comparison with approx. 85% for experiment and the $T = 0.5$ model). This shows that the larger cohesive forces favor demonstrably larger patches in that 25% of the patches are larger than 10 mm^2 for the $T = 0.6$ model vs. 15% from experiment and the $T = 0.5$ model. Second, the patches become smaller for the later regeneration cycles; the opposite tendency (patches became larger) was observed in the early version of the model where the cohesive bonds were healed. This decrease in patch size can also be seen in Fig. 10. Fig. 10 displays the median patch size A_{50} vs. cycle number.

There is very good agreement of the curves for cycles 4 and higher; for low cycle numbers the patches obtained

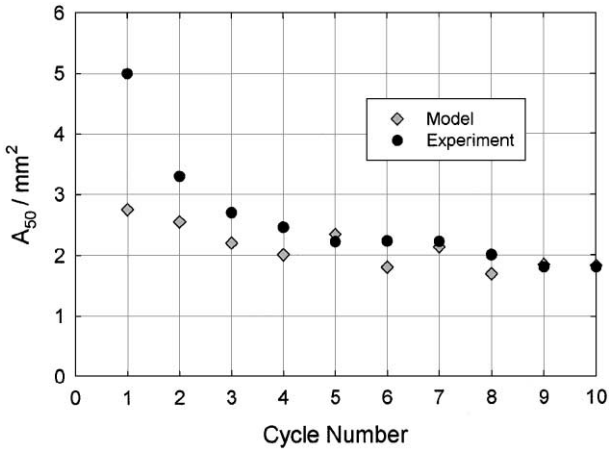

Fig. 10. Median size A_{50} of the patches from both the experiment and the model.

from experiment are larger than those given from modelling; this might be due to the conditioning of the filter medium, and might be related to the larger regeneration efficiency (Fig. 6) for the first two cycles. For cycles 4 and higher, the median patch size (where the cumulative distribution is 50% Fig. 9b) from modelling is approximately (5 blocks) × (0.4 mm^2/block) = 2 mm^2. This is very close to the median size from the experimental distribution (Fig. 9a).

Because the overall regeneration efficiency is nearly constant over a number of filtration cycles but the patches are becoming smaller with increasing number of the filtration cycle the number of patches needs to grow. Fig. 11 gives the number of patches per unit filter area vs. cycle number.

There are significant differences (up to 40%) between modelling and experiment for the patch number density (number of patches per unit area). After the tenth regeneration cycle, the filter coupon (area 154 cm^2) has about 2.6

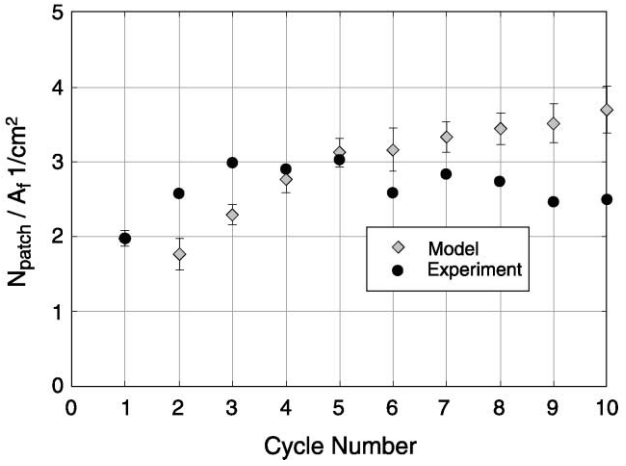

Fig. 11. Number density of the cleaned patches from both the experiment and the model.

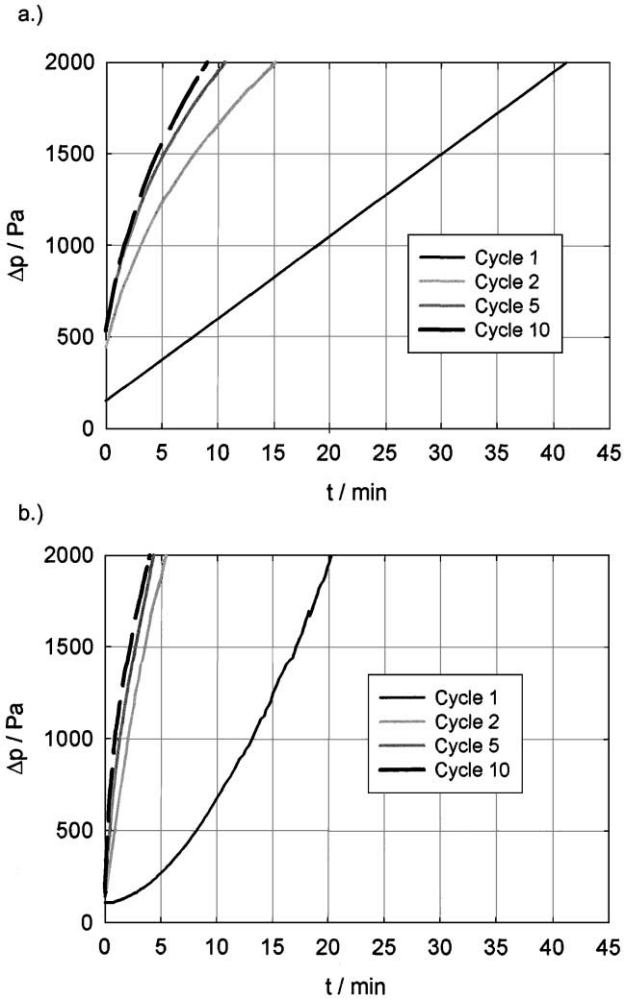

Fig. 12. (a) Pressure drop vs. time during filtration cycles #1, #2, #5, and #10 from modelling and (b) from experiment.

patches per cm^2, while the model system has a patch density of 3.6 patches per cm^2. The modelling suggests that the number of patches increases with cycle number, but the experiments show nearly constant behaviour for later cycles. It seems plausible that this failure of the model may be related to the artificial square gridding of the model in that no removed patch can be smaller than 1 block (0.4 mm^2). That is, since the fraction of the surface removed (approx. 28%) and the median patch size (approx. 2 mm^2) are approximately the same in the model and in the experiment, and since both show a small decrease in median size with cycle number, the experimentally observed increase (Fig. 9a) in the fraction of very small sizes and the corresponding decrease in the fraction of large sizes (20 mm^2) are to be contrasted with the model having a negligible change in the fraction of single block patches (Fig. 9b) and a pronounced decrease in the fraction of very large patches. Because of this pronounced decrease in the fraction of very large patches, (100 mm^2) a larger number of patches will be needed in the modelling to maintain the same regeneration efficiency.

4.4. Operating behaviour

As discussed elsewhere (e.g., Ref. [11]), the regeneration behaviour has a major influence on the operational behaviour of the filtration process and hence on the dust cake build-up. The operational behaviour can be characterized by the pressure drop curve and its dependence on the filter cycle number.

4.4.1. Pressure drop curves

Fig. 12 gives the pressure drop vs. filtration time for cycles 1, 2, . . ., 10 obtained from our model (a) and from experiment (b). The factor, η, in Eq. (10) is the fourth adjustable parameter; this determines the time scale in the modelling. It can be seen from Fig. 12a that the pressure drop curve is linear in the first filtration cycle, whereas the experiment (Fig. 12b) gives a progressive increase of pressure drop in cycle 1. This is due to dust cake compression, as will be shown. The residual pressure drops predicted from modelling are higher than the measured ones. This is obviously due to the neglect of cross-flow in the filter medium, as discussed by Dittler and Kasper [13].

In the model, the pressure drop curves for cycles 2, 5 and 10 have a convex shape, which is due to incomplete filter regeneration (e.g., Ref. [12]) whereas the cycle-to-cycle differences in the shape of the curves depend on the local frequency of regeneration [30]. Basically the same tendencies are observed experimentally, only the shape of the pressure drop curves is not as convex as predicted by the modelling. This is also an effect of dust cake compression.

The effect of dust cake compression has a significant influence on the operational performance of the filtration process. Fig. 13 gives a comparison of pressure drop curves of cycle 2 as obtained experimentally and from the modelling.

The model neglecting dust cake compression and cross-flow in the filter medium gives a higher residual pressure

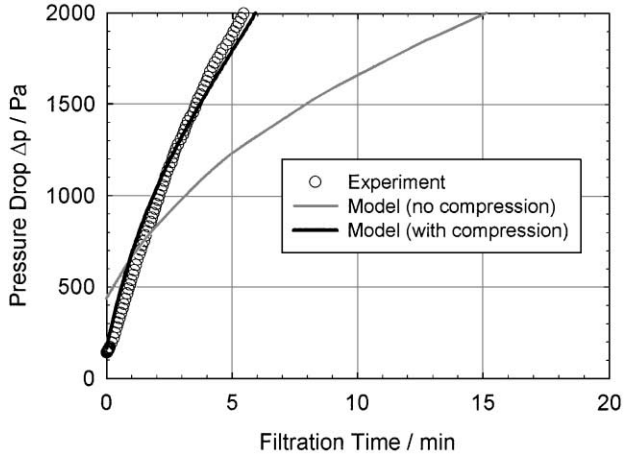

Fig. 13. Effect on the filtration pressure curves of including filter cake compression in the modelling.

drop and a higher filtration time. The shape of the pressure drop curve is convex, as expected from calculations discussed in Ref. [12]. When accounting for cross-flow inside the filter medium the residual pressure drop is close to the pressure drop of the new filter medium [13]. Dust cake compression influences the shape of the pressure drop curve and hence the filtration time significantly. The pressure drop curve is not as convex as predicted by the model. Dust cake compression increases the resistance to flow of the dust cake and hence influences the shape of the pressure drop curve and the filtration time. The compression of the dust cake was described by a pressure drop-dependent resistance to flow of the dust cake in accordance with an earlier publication by Schmidt [31].

4.4.2. Dust cake heights

Dust cake compression also influences the dust cake height. This can be seen from Fig. 14.

Fig. 14 gives the dust cake height distribution before the 10th filter regeneration as obtained experimentally and from the modelling. The dust cake height distribution obtained experimentally has a much steeper increase than the dust cake height distribution from the modelling. Because of the higher resistance to flow of dust cake in the uncleaned regions, in the actual experiments the dust cake grows less in the unregenerated filter areas and more in the regenerated filter areas than is predicted by the model, thereby explaining the differences in the dust cake height distributions. Besides the effect of K_2' and its pressure drop dependence, dust cake height is mainly influenced by the porosity of the dust cake (Eqs. (3) and (4)). In the model we assumed a constant porosity of $\varepsilon = 0.8$, whereas the actual porosity depends on the dust cake height because of compression phenomena [31], which, themselves have a direct influence on the dust cake height. To quantify these phenomena in detail, further investigations need to be performed.

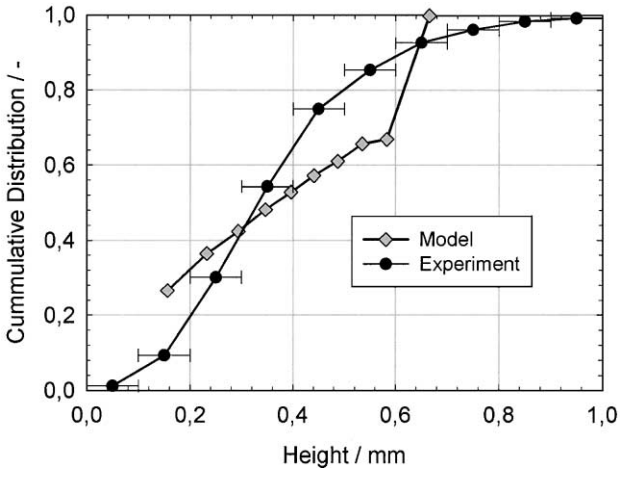

Fig. 14. Dust cake height distribution before 10th filter regeneration.

5. Conclusion

Patchy cleaning is widely observed when gas cleaning filter media are regenerated incompletely. In order to investigate the filter regeneration behaviour and its influence on the operational performance of rigid filter media over a series of filtration cycles, experiments were performed in a filter test rig built in accordance with German VDI guideline 3926. This test rig was equipped with a measuring system capable of measuring the dust cake height on the filter medium surface with a high lateral and topographical resolution. With this measuring system, information about the overall regeneration efficiency, the local frequency of regeneration, and the number and size of regenerated areas was obtained over a series of filtration cycles. The modelling results were compared to the experimental results.

The original two-dimensional grid model was developed to study layer removal during the first cycle [17–22]. In accounting for adhesive, as well as cohesive properties of the dust cake, this model produced results in good agreement with experiment [16]. For the present work, we extended the model to a series of cycles by using a simple rule for depositing the filter cake on a patchily cleaned surface. This deposition rule neglected cross-flow and filter cake compression in assuming that the flow velocity through any given block is proportional to the thickness of the constant-porosity filter cake of that block. As discussed in Section 4, use of only four adjustable parameters in this version of the model produced results in good agreement with the comprehensive set of experiments.

Achieving this level of agreement with the room-temperature experiments necessitated the assumption that any adhesive or cohesive bond broken during a regeneration cycle was not reformed during subsequent filtration cycles. If the model restored the adhesive bonds between uncleaned patches of filter cake and the filter, essentially the same patches were removed during each regeneration, which is in striking disagreement with the experimental frequency of regeneration (Fig. 8a). If the model restored the cohesive bonds between uncleaned blocks of filter cake, (i) the patch size increased from cycle to cycle in disagreement with experiment (Figs. 9a and 10); (ii) too many of the same blocks were removed every time in disagreement with the experimental frequency of regeneration (Fig. 8a); and (iii) after the first cycle, the filtration pressure decreased from cycle to cycle in disagreement with the experimentally observed increase (Fig. 12b). Therefore, the model development was guided by our extensive experimental results. Consequently, the modelling indicates that in these experiments bonds only form between newly deposited particles in the filter cake, and that once these bonds are broken, they do not re-heal. Of course, different filtration parameters (more reactive dust particles and elevated temperatures) may lead to different conclusions. However, the present work provides a frame-

work in which to investigate these issues and to form a predictive model of the filtration process.

Our results indicate (i) that filter conditioning, especially after the first few regeneration steps, influences the structures of patchy cleaning, and (ii) that dust cake compression has a major influence on the operational performance of the filtration process. We showed that because of filter cake compression, the shape of the pressure drop curve is more linear and the dust cake height is significantly lower in experiment than the modelling predicts.

In future modelling work, we plan to improve the filter cake deposition component of our modelling by accounting for the height and porosity effects of filter cake compression as well as for cross-flow. We also plan to investigate the effects of adjusting other parameters: e.g., the fraction of cohesive bonds that may be restored as well as the fraction of adhesive bonds that are restored. In addition, we will study the effect of larger pressure pulses, increased thickness, and a narrower distribution of adhesive strengths.

List of Symbols

A_f	Filter surface area (m^2)
A	Patch size (mm^2)
A_{50}	Median patch size (mm^2)
$\varepsilon(i,j)$	Displacement of (i,j) block**
ε	Porosity (–)
F	Backpulse pressure force *
γ	Factor (–)
i	x-Position in the grid**
j	y-Position in the grid**
k^a	Adhesive spring constant *
k^c	Cohesive spring constant *
K_1'	Specific resistance to flow of filter medium (Pa* s/m)
K_2'	Specific resistance to flow of dust cake (s^{-1})
ℓ	Size scale of model block (mm)
N	Number of patches (–)
n	Number of filtration cycle (–)
η	Volume of filter cake/volume of flow (–)
ΔP	Pressure drop*
R	Dimensionless ratio of flow resistances (–)
r_c	Resistance of flow of dust cake (Pa)
r_f	Resistance of flow of filter medium (Pa)
ρ_s	Density of dust (kg/m^3)
S^a	Strength of adhesive bond*
S^c	Strength of cohesive bond*
T	Thickness parameter (–)
t	Time (s)
v	Filtration velocity (cm/s)
v	Dimensionless filtration velocity (–)
W	Areal mass loading (kg/m^2)
x	Position**
y	Position**

* In the model, all forces, strengths and spring constants are measured relative to the average adhesive force which has the dimensionless value of 1/2. To compare with real systems, one needs to find the factor which converts from dimensionless 1/2 to the real, average adhesive strength of the system (see Ref. [16]); all forces, strengths and spring constants will then scale by this same factor.

** In the model, all distances are in units of the length scale factor ℓ.

Acknowledgements

Martin Ferer gratefully acknowledges the support of the U.S. Department of Energy, Office of Fossil Energy. Achim Dittler and Gerhard Kasper thank the German Science Foundation (DFG) for financial support of their work.

References

[1] D. Koch, J.P.K. Seville, R. Clift, Powder Technol. 86 (1996) 21–29.
[2] W. Duo, N.F. Kirkby, J.P.K. Seville, R. Clift, Chem. Eng. Sci., 52 (1) (1997) 141–151.
[3] W. Duo, J.P.K. Seville, N.F. Kirkby, H. Büchele, C.K. Cheung, Chem. Eng. Sci. 52 (1) (1997) 153–164.
[4] J.P.K. Seville, W. Cheung, R. Clift, Filtr. Sep. (May/June 1989) 187–190.
[5] K. Morris, R.W.K. Allen, R. Clift, Filtr. Sep. (January/February 1987) 41–45.
[6] T. Pilz, F. Löffler, Chem. Eng. Technol. 67 (1995) 745–749.
[7] T. Pilz, F. Löffler, Preprints Filtec Conference, Karlsruhe, 1995, pp. 139–148.
[8] Ch. Stöcklmayer, W. Höflinger, Filtr. Sep. (May 1998) 373–377.
[9] Ch. Stöcklmayer, W. Höflinger, Math. Comput. Simul. 46 (1998) 601–609.
[10] A. Dittler, B. Gutmann, R. Lichtenberger, H. Weber, G. Kasper, Powder Technol. 99 (2) (1998) 177–184.
[11] A. Dittler, G. Kasper, Patchy Cleaning of Rigid Filter Media, World Filtration Congress 8, Brighton, U.K., 3.–7, April 2000, Proceedings, vol. I, 2000, pp. 333–336.
[12] A. Dittler, G. Kasper, Chem. Eng. Process. 38 1999, pp. 321–327.
[13] A. Dittler, G. Kasper, High Temp. Gas Cleaning, Pub. Inst. für Mechanisches Verfahrenstechnik und Mechanik, Universität Karlsruhe, Karlsruhe, Germany, Sept. 1999, pp. 119–127.
[14] A. Dittler, G. Kasper, High Temp. Gas Cleaning, Pub. Inst. für Mechanisches Verfahrenstechnik und Mechanik, Universität Karlsruhe, Karlsruhe, Germany, Sept. 1999, pp. 164–171.
[15] E. Schmidt, Chem. Eng. Technol. 21 (1988) 26–29.
[16] M.V. Ferer, D.H. Smith, Chem. Eng. Sci. 55 (21) (2000) 5003–5011.
[17] M.V. Ferer, D.H. Smith, Phys. Rev. E 58 (1998) 7071–7078.
[18] M. Ferer, D.H. Smith, J. Appl. Phys. 81 (1997) 1737–1744.
[19] M. Ferer, D.H. Smith, Phys. Rev. E 57 (1998) 866–874.
[20] M. Ferer, D.H. Smith, Aerosol Sci. Technol. 29 (1998) 246–256.
[21] M. Ferer, D.H. Smith, Phys. Rev. E 58 (1998) 7071–7078.
[22] M. Ferer, D. Smith, High Temp. Gas Cleaning, Pub. Inst. für Mechanisches Verfahrenstechnik und Mechanik, Universität Karlsruhe, Karlsruhe, Germany, Sept. 1999, pp. 172–184.
[23] H.J. Hermann, S. Roux, Statistical Models for the Fracture of Disordered Media, North Holland, Amsterdam, 1990.
[24] P. Meakin, Science 252 (1991) 226–234.
[25] P.M. Duxbury, P.L. Leath, P.D. Beale, Phys. Rev. B 36 (1987) 367–380.
[26] VDI Richtlinie 3926- Band 6, 1994.

[27] R. Klingel, VDI Z., Fortschr.-Ber. Reihe 3 Verfahrenstechnik 76 (1982).
[28] W. Cheung, PhD dissertation, University of Surrey, Guilford, U.K., 1989.
[29] C. Kanaoka, T. Kishima, M. Furuuchi, in: Schmidt, Gäng, Pilz, Dittler (Eds.), High Temperature Gas Cleaning, 1996, pp. 183–192.
[30] A. Dittler, G. Kasper, Presentation at the GVC Fachausschuß "Gasreinigung" Würzburg, Germany, 2000.
[31] E. Schmidt, Staub-Reinhalt. Luft 53 (1993) 369–376.
[32] D.H. Smith, G. Ahmadi, et al., Powder Technol. 94 (1997) 15–21.
[33] D.H. Smith, G. Ahmadi, et al., Aerosol Sci. Technol. 29 (1998) 224–235.